Sergey Y. Yurish
Editor

Advances in Networks, Security and Communications: Reviews

Volume 2

Advances in Networks, Security and Communications: Reviews,

Volume 2

Sergey Y. Yurish
Editor

Advances in Networks, Security and Communications: Reviews

Volume 2

International Frequency Sensor Association Publishing

Sergey Y. Yurish
Editor

Advances in Networks, Security and Communications: Reviews
Volume 2

Published by International Frequency Sensor Association (IFSA) Publishing, S. L., 2019
E-mail (for print book orders and customer service enquires): ifsa.books@sensorsportal.com

Visit our Home Page on http://www.sensorsportal.com

ISBN: 978-84-09-14510-2
e-ISBN: 978-84-09-14509-6
BN-20191130-XX
BIC: TJK

Acknowledgments

As Editor I would like to express my undying gratitude to all authors, editorial staff, reviewers and others who actively participated in this book. We want also to express our gratitude to all their families, friends and colleagues for their help and understanding.

Contents

Chapter 9
Localization in GPS Denied Environment

Heng Zhang, Siwen Chen, Chee Kiat Seow and Soon Yim Tan

9.1. Introduction

Wireless localization is important in Emergency 911 subscriber safety service and sensor network applications, such as indoor navigation and surveillance [1-3] as more people spend more and more time in indoor environment. However, the Global Navigation Satellite System (GNSS) is hard to achieve satisfactory localization accuracy in indoor area due to the serious attenuation and multipath fading of the GPS (Global Positioning System) signal by walls and furniture [4-6]. The design of indoor localization system is required.

Such systems attempt to locate the mobile device (MD) by measuring the radio signals travelling between the MD and a set of reference devices (RDs) with known positions. The measured parameters can be related to the time of arrival (TOA) [7-9], angle of arrival (AOA) [10] and signal strength of the received signal or combination of these [11].

TOA and AOA based techniques require at least three and two RDs in Line-of-Sight (LOS) with MD respectively in a 2D environment. In our earlier work, we have proposed various techniques to find the MD location by leveraging on LOS path between any RD and MD pair [12-14]. However, in an indoor environment, LOS path may not exist and the received signal will be dominated by many NLOS paths [15]. The location error will be increased greatly if these NLOS paths are mistakenly used for localization. To solve this issue, many localization algorithms have been proposed which can be divided mainly into two categories. One category is focusing on mitigating the NLOS error by using weight method to minimize the contribution of NLOS RDs which turns out not reliable [16-18]. Another category is focusing on detecting the NLOS RDs then discarding them which will result in insufficient RD issue [19, 20] in dense multipath environment. Therefore, the indoor localization algorithms using LOS path only result in either low accuracy or insufficient RD issue.

Heng Zhang
School of EEE, Nangyang Technological University, Singapore

Recently, localization schemes that are able to locate MD by using NLOS paths directly have been reported [21, 22]. In [21], Taylor series methodology is applied to find the MD location by means of initial guess of MD location and single bounce paths. In [22], the MD location can be determined if there exists at least two dominant NLOS paths without the need for initial estimation of MD location.

The objective of this chapter is twofold. Firstly, a novel method is presented to significantly improve the localization accuracy by using the concept of virtual RD (VRD) to determine MD location. The position of virtual RD for a given NLOS path can be determined by initial guess of the MD location [21]. Alternatively, the VRD location can also be found if the MD transits from LOS to NLOS region. After the positions of all VRDs are identified, the subsequent MD location can be determined by using just one dominant NLOS path and its corresponding VRD. The second objective of this chapter is to overcome the limitation of the earlier presented VRD based localization. The VRD based localization [23] does not mention how to match the estimated VR with the measured one-bound path and it requires both transceivers with the ability of measuring TOA and AOA. Furthermore in [24-26], various VRD based indoor localization algorithm with the knowledge of the layout map, where the location of VRs could be pre-calculated, are also developed. The difference is in [24], the algorithm jointly using TOA and AOA information measured at multiple RDs to reduce the multi-modal uncertainties of MD and this research only give simulation result. On the other hand, in [25] and [26], these algorithms either using tracking or measuring at multiple RDs to reduce the uncertainties with TOA information only. In [27], a simultaneous target and multipath positioning (STAMP) scheme based on joint TOA and AOA measurement is proposed. The multiple bounds paths are discarded by using multi-hypothesis data association. However, in some environment, like the enclosed meeting room, the multiple bounds will exist all the time and cannot be discarded.

The second portion of this chapter presented an indoor VRD based TOA localization algorithm with the knowledge of environment layout. With the help of the layout map of the environment, the location of VRDs can be pre-calculated according to the multipath propagation model. The first step of the proposed algorithm involves estimation of the data association matrix through a least square (LS) estimator which is different with the conventional maximum likelihood (ML) or maximum a posteriori (MAP) estimator. The second step is using the associated observation data and paths to estimate the location of MD through weighted least square (WLS) method mentioned in [16]. To solve the multi-modal issue, the algorithm utilizes multiple RDs and centroid method. Due to some modals of MD are symmetric with the perpendicular bisector of any two VRs, by using multiple RDs placed unsymmetrically with the perpendicular bisector could mitigate the multi-modal issue. Furthermore, using the centroid of the minimum H number of square residual modals to estimate the data association matrix, the modals with very small square residual but far away from the MD could be pushed nearer to the vicinity of MD to mitigate the multi-modal issue.

9.2. Estimation of Virtual Reference Device

Fig. 9.1(a) illustrates the geometrical relationship between RD, MD and a virtual RD which is associated with a one bounce reflection path. RD has a known location (x_R, y_R) with measured data AOA θ. MD has an unknown location (x, y) with measured data AOA ϕ. $\hat{M}D$ is the estimated MD position through the initial guess using Taylor Series Methodology [21] or using the available LOS measurement metrics [11, 12, 18, 21, 22]. The measurement data TOA t is related to the propagation distance using $d = ct$ where c is the speed of wave propagation. The TOA (distance *d*) and AOA measurement values are assumed to be perturbed by Gaussian noise:

$$\theta = \theta^0 + n_\theta, \phi = \phi^0 + n_\phi, d = d^0 + n_d, \quad n_\beta = N(0, \sigma_\beta) \quad \beta = \theta, \phi, d, \tag{9.1}$$

where θ^0, ϕ^0 and d^0 are the true TOA and AOA values of signal path, and n_θ, n_ϕ and n_d denote the zero mean Gaussian random noise with standard deviation σ_β.

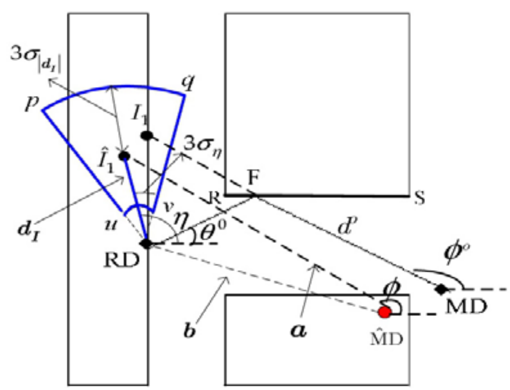

Fig. 9.1(a). Position of virtual RD originated from RD.

As shown in Fig. 9.1(a), I_1 is the true virtual RD of signal path RD-F-MD due to reflection at surface RS. $\hat{I}_1$ is the estimated value of I_1. The position of virtual RD can be constructed from RD with the vector $\boldsymbol{d}_I = |\boldsymbol{d}_I| \angle \eta$ where $\eta = (\theta + \phi)/2$. $|\boldsymbol{d}_I|$ is the distance between RD and $\hat{I}_1$ which can be written as:

$$|\boldsymbol{d}_I|^2 = \boldsymbol{a}^{\mathrm{T}}\boldsymbol{a} + \boldsymbol{b}^{\mathrm{T}}\boldsymbol{b} - 2\boldsymbol{a}^{\mathrm{T}}\boldsymbol{b}, \tag{9.2}$$

where $\boldsymbol{a} = |\boldsymbol{a}| \angle \phi$ and $\boldsymbol{b} = \boldsymbol{RD} - \hat{\boldsymbol{M}}\boldsymbol{D}$. $|\boldsymbol{a}|$ is the distance between $\hat{M}D$ and $\hat{I}_1$, approximately equal to the measured TOA (distance) due to the signal path RD-F-MD. The position of virtual RD originated from RD can be constrained to an enclosed region, *uvqp*, with angle and distance measured from RD within $\left[\eta-3\sigma_{\eta},\eta+3\sigma_{\eta}\right]$ and $\left[\left|d_I\right|-3\sigma_{|d_I|},\left|d_I\right|+3\sigma_{|d_I|}\right]$, where $\sigma_{\eta}=(\sigma_{\theta}+\sigma_{\phi})/2$ and $\sigma_{d_I}=\sigma_d\left|\boldsymbol{d}_I\right|/\left|\boldsymbol{a}\right|$ as depicted in Fig. 9.1(a)

Similarly, the position of virtual RD originated from $\hat{M}D$ can be constructed within $\left[\phi-3\sigma_{\phi},\phi+3\sigma_{\phi}\right]$, $\left[\left|\boldsymbol{a}\right|-3\sigma_d,\left|\boldsymbol{a}\right|+3\sigma_d\right]$ that is, *eghi*, as shown in Fig. 9.1(b).

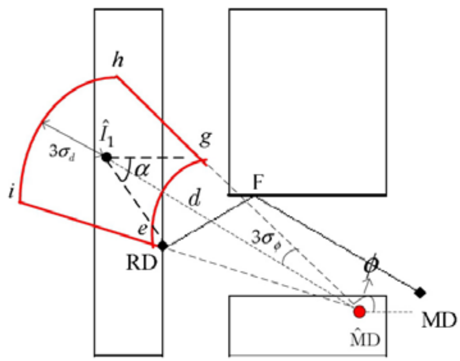

Fig. 9.1 (b). Position of virtual RD originated from $\hat{M}D$.

The estimated virtual RD is determined from the N vertices of the intersections of the two earlier obtained virtual RD regions, *abfmnr*, as shown in Fig. 9.1(c). Without the loss of generality, a is chosen as (x_1, y_1) and r as (x_N, y_N). The coordinates of the N (N = 6 in this case) vertices are ordered clockwise from a, (x_1, y_1) to r, (x_N, y_N). To determine $\hat{I}_1$ using weighted least square distance methodology [28], the intersection area is divided into a set of N-2 triangles using a as a reference. In this case, there will be four triangles namely *abf, afm, amn* and *anr*. J is the weighted least square distance to all the triangular centroid points, which is defined as

$$J=\sum_{\mathrm{j}=1}^{N-2} w_j\left(\left(x_{cj}-x_I\right)^2+\left(y_{cj}-y_I\right)^2\right), \tag{9.3}$$

where $\left(x_I,y_I\right)$ is the location of $\hat{I}_1$, $\left(x_{cj},y_{cj}\right)$ is the centroid of the j^{th} triangular. w_j is the weighting factor which is chosen to be proportional to the area of the j^{th} triangle. (9.3) can be re-arranged in matrix form as

$$J=\left(\mathbf{H}\hat{\mathbf{I}}_1-\mathbf{C}\right)^{\mathrm{T}}\mathbf{W}\left(\mathbf{H}\hat{\mathbf{I}}_1-\mathbf{C}\right), \tag{9.4}$$

where $\mathbf{C}$ is the coordinate of all triangular centroids given as $\mathbf{C} = \left[\mathbf{c}_1, \cdots \mathbf{c}_j, \cdots \mathbf{c}_{N-2}\right]^{\mathrm{T}} = \left[x_{c1}, y_{c1}, \cdots x_{cj}, y_{cj}, \cdots x_{cN-2}, y_{cN-2}\right]^{\mathrm{T}}$. $\mathbf{H} = \left[\mathbf{h}_1, \mathbf{h}_2, \cdots \mathbf{h}_j \cdots \mathbf{h}_{N-2}\right]^{\mathrm{T}}$ and $\mathbf{h}_j = \mathbf{I}_{2\times 2}$, a 2×2 identity matrix.

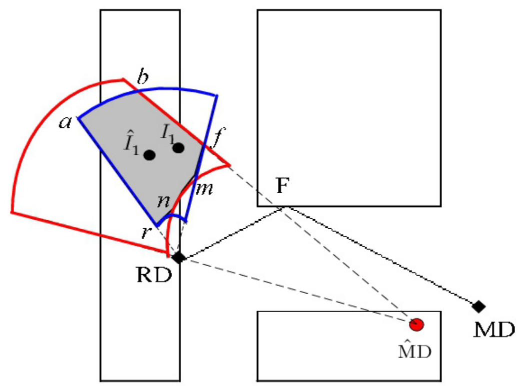

Fig. 9.1(c). Intersection of virtual RD regions.

$$\mathbf{W} = \frac{1}{\sum_{k=1}^{N-1} \det(\boldsymbol{P}_k) + \begin{vmatrix} x_N & y_N \\ x_1 & y_1 \end{vmatrix}} \mathrm{diag}(\boldsymbol{B}_1 \cdots \boldsymbol{B}_j \cdots \boldsymbol{B}_{N-2}),$$

where $\boldsymbol{P}_k = \begin{bmatrix} x_k & y_k \\ x_{k+1} & y_{k+1} \end{bmatrix}$, $\boldsymbol{B}_j = \mathrm{diag}(\det(\boldsymbol{S}_{j+1} \times \boldsymbol{S}_{j+2}), \det(\boldsymbol{S}_{j+1} \times \boldsymbol{S}_{j+2}))$, $\boldsymbol{S}_{j+1} = \left[x_{j+1} - x_1 \quad y_{j+1} - y_1\right]$, and $\boldsymbol{S}_{j+2} = \left[x_{j+2} - x_1 \quad y_{j+2} - y_1\right]$. Finally, the estimated virtual RD $\hat{I}_1$ corresponding to the NLOS path RD-F-MD can be calculated using

$$\hat{\mathbf{I}}_1 = \left[x_I \ y_I\right]^{\mathrm{T}} = \arg\left\{\min J\right\} = \left(\mathbf{H}^{\mathrm{T}} \mathbf{W} \mathbf{H}\right)^{-1} \mathbf{H}^{\mathrm{T}} \mathbf{W} \mathbf{C} \tag{9.5}$$

The virtual RDs for other NLOS paths can be determined similarly. When MD moves to a new location, the virtual RD that corresponds to the dominant NLOS path at new location can be identified by using measured TOA and AOA of that path. Based on the measured TOA, AOA and the corresponding virtual RD, new MD position can be determined as:

$$\hat{\mathbf{M}}\mathbf{D} = \left[x \ y\right]^{\mathrm{T}} = \hat{\mathbf{I}}_1 + \mathbf{D} = \left(\mathbf{H}^{\mathrm{T}} \mathbf{W} \mathbf{H}\right)^{-1} \mathbf{H}^{\mathrm{T}} \mathbf{W} \mathbf{C} + \mathbf{D}, \tag{9.6}$$

where $\mathbf{D} = \left[d\cos([\phi-\theta]/2+\alpha) \quad d\sin([\phi-\theta]/2+\alpha) \right]^{\mathrm{T}}$ is the measured path vector due to dominant NLOS path with $\alpha = \tan^{-1}[(y_R - y_I)/(x_R - x_I)]$ (see Fig. 9.1(b)). At each MD location, all virtual RDs will be recalculated. It is noteworthy that (9.6) only requires measured TOA and AOA to estimate the MD location. It does not require prior knowledge of the location, orientation and nature of the obstacles in the environment.

9.3. Simulation and Experimental Results for VRD Based Localization

To check the accuracy and robustness of our proposed localization scheme, simulation and experiment will be carried out in an indoor environment with dimension 16.4 m × 9.5 m along X and Y axis such that $0 \le x \le 16.4$ m and $0 \le y \le 9.5$ m. This dimension also corresponds to Internet of Things (IoT) laboratory at School of EEE, Nanyang Technological University (NTU) as shown in Fig. 9.2. In this simulation, the RD is fixed at (12.9 m, 0.7 m) with 5,000 uniformly distributed MD locations. The obstacles are assumed to be randomly distributed with the probability of NLOS path assumed to be $1-e^{-r/\lambda}$ [15] where r is the direct distance between RD and MD, while λ is the mean distance from RD to obstacles. λ is chosen to be 5 m and 10 m [15] which translates to NLOS path's probability of 70 % and 45 % respectively. Distance standard deviation is assumed to be 2 m. Angle standard deviations vary from 1º to 10º [22].

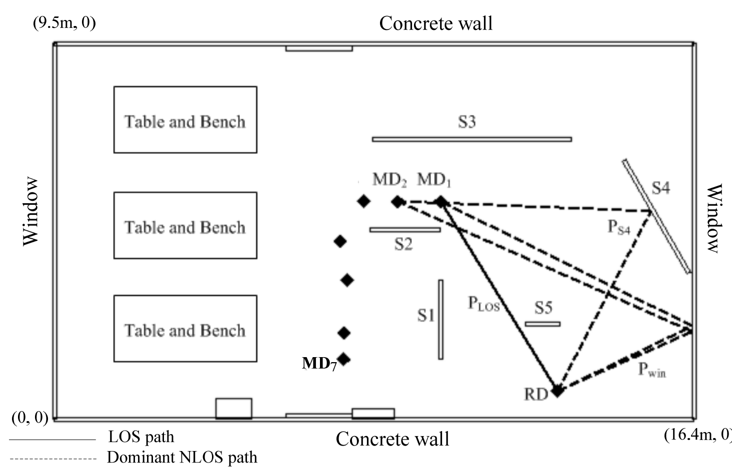

Fig. 9.2. Geometry of IoT laboratory at School of EEE, NTU.

Fig. 9.3 depicts the average location error (ALE) performance by comparing our proposed localization scheme with the existing NLOS localization schemes in [21] and [22]. Comparison is also made with conventional TOA/AOA and TOA localization schemes with their NLOS mitigation techniques in [19] and [18], respectively. Because [18] and [19] require at least two and three RDs respectively, another three RDs are placed symmetrically at (3.5 m, 0.7 m), (3.5 m, 8.8 m) and (12.9 m, 8.8 m) near the other three corners. In other word, [18] and [19] will use four RDs to perform localization. In our proposed localization scheme and [21], the initial MD location is assumed to be randomly distributed within a circle centered at MD location with radius equal to 5 % of the distance between RD and MD [21-22]. As shown, our proposed NLOS localization technique based on one RD achieves an ALE of less than 2 m under both cases: λ = 5 m and 10 m, outperforming all existing localization schemes. Cong and Zhuang [19] achieves the ALE of 8.7 m and 6.5 m, while Jia and Buehrer [18] has the ALE 8.5 m and 6.1 m for λ = 5 m and 10 m, respectively. Seow and Tan [22] and Li et al. [21] are not shown as the ALE are more than 15 m. The reason is that in [22], the accuracy will be seriously degraded when the angle between the obstacles is very small whereas in [21] the Taylor series methodology only works well when there is a good initial guess and small measured parameters' standard deviation.

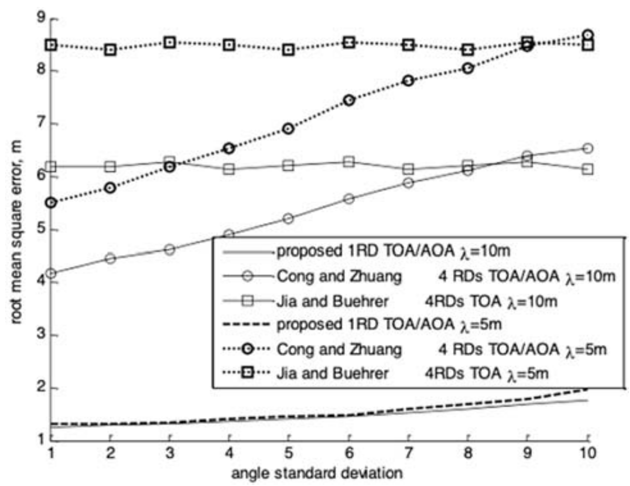

Fig. 9.3. ALE performance comparisons.

To test the performance of our proposed localization scheme in a real environment, experiment is conducted at IoT laboratory. There are glass windows, concrete walls and five dominant metallic obstacles, namely S1, S2, S3, S4 and S5 as shown in Fig. 9.2. In the experiment, RD is fixed at (12.9 m, 0.7 m) while MD moves from MD_1 to MD_7. MD_1 and MD_7 are in LOS and the rest are in NLOS condition. The experiment is carried out using vector network analyzer (VNA) with frequency sweep from 2 to 3 GHz over 1601 frequency points. A 4×4 virtual antenna array with element spacing of 5 cm that corresponds to half a wavelength at 3 GHz is used at both RD and MD. At each MD location, 16 S21 measurement data for each frequency point is used to obtain the average. Using the average data, TOA and AOA of two dominant paths at each MD location will be calculated by parameter estimation EM algorithm [29]. The EM algorithm can extract the TOA and AOA of the signal path as long as its signal is above the threshold. These values are used to determine MD location using equation (9.6). Root mean square (RMS) error pertains to the actual MD location is given as $\sqrt{(x-x^0)^2+(y-y^0)^2}$, where (x^0, y^0) and (x, y) are the true and estimated MD location respectively.

Based on the TOA and AOA data that obtained from the average of 16 measurement data at each of the 7 location points, the angles standard deviation of the dominant paths at both RD and MD are found to be 5.1° and 7.0° respectively. Distance standard deviation is found to be 0.51 m. Table 9.1 shows the localization RMS error comparison of the proposed localization scheme with existing NLOS localization schemes [21-22]. The average RMS error of our proposed localization scheme for the 7 location points is calculated to be 1.6 m as compared to the average RMS error of 21.3 m and 8.6 m in [21] and [22] respectively. At each MD location, we can identify whether the dominant NLOS path undergoes one or multiple reflections by checking the measured distance and angle satisfy the triangular relationship of a single bounce path.

Table 9.1. Comparison of RMS error (m) from MD1 to MD7.

	MD_1	MD_2	MD_3	MD_4	MD_5	MD_6	MD_7
Proposed scheme	0.34	0.26	0.48	2.87	3.05	3.66	0.84
Seow and Tan [22]	0.62	0.4	0.57	4.04	14.9	38.7	1.22
Li et al. [21]	0.34	0.35	46.6	47	37	17	0.76

Table 9.2 shows the correlation of parametric estimation based on EM algorithm and ray tracing methodology [30] at MD_1 and MD_2. At MD_1 the dominant paths are LOS path (P_{LOS}) and one reflected path from window (P_{win}), whereas at MD_2 there are two one reflected paths from window and S4 (P_{win} and P_{S4}). As shown, the propagation paths simulated using ray tracing are well correlated with measured paths in the experiment. Thus, we can use the data metrics from the ray tracing methodology and add Gaussian noise statistically to evaluate the performance of our proposed localization scheme. The true TOA and AOA of each signal path between RD and MD are subjected to Gaussian noise with zero mean and known standard deviation. RMS error is calculated for 5,000 simulation runs. To compare with [18] and [19], another three RDs are placed at the same positions as the one in the ALE performance result.

Table 9.2. Correlation between EM Algorithm [29] and Ray Tracing [30].

	Extracted path from measured data (d, ϕ θ)			**Ray traced path (d, ϕ θ)**
MD_1	6 m	302°	122.9°	P_{LOS} (5.7 m, 302°, 122°)
	11.1 m	334°	25°	P_{win} (11 m, 334°, 26°)
MD_2	12 m	335°	21°	P_{win} (12 m, 336°, 24°)
	11.7 m	359°	61°	P_{S4} (11.7 m, 358°, 62°)

Fig. 9.4 depicts the accuracy of proposed localization scheme and makes comparison with existing localization schemes in terms of cumulative distribution function when MD

transits from LOS condition at MD_1 (9.9 m, 5.5 m) to NLOS at MD_2 (8.8 m, 5.5 m). At MD_1, first dominant LOS path is exploited to estimate the MD [9]. After MD location has been estimated, the virtual RD corresponding to the NLOS path P_{win} can be determined. When MD moves to the next position MD_2, based on equation (9.6), we are able to use the calculated virtual RD associated with P_{win} and the new measured data (TOA and AOA) at MD_2 to estimate MD_2 location. As shown in Fig. 9.4, our proposed localization scheme using one reflection path outperforms the existing localization schemes. For example, under σ_d = 1 m, $\sigma_\theta = \sigma_\phi$ = 5°, our proposed localization scheme achieves the accuracy of 2.3 m for 90 % of the time as compared with 3.6 m and 4.5 m in [22] and [19] respectively. The margin of improvement are 36 % and 49 % respectively.

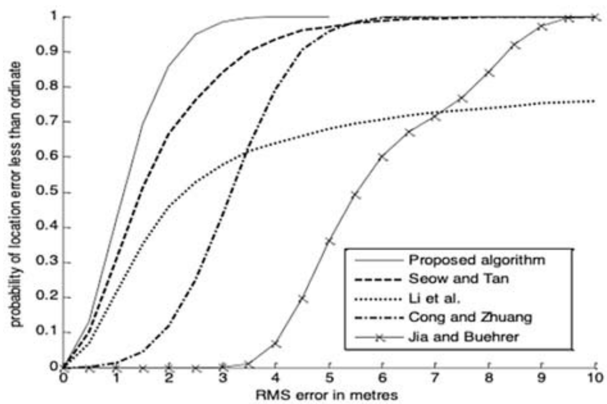

Fig. 9.4. Comparison of cumulative distribution function (CDF) performance for MD_2 at (8.8 m, 5.5 m) under $\sigma_d = \sigma_r$ = 1 m, $\sigma_\theta = \sigma_\phi$ = 5°.

9.4. Theory and Formulation for VRD TOA Localization Algorithm

9.4.1. Environment, Channel Response and Multipath Model

Previous section presented a NLOS localization scheme based on the concept of VRD. Simulation and experimental results have shown that the proposed NLOS localization scheme using one RD outperforms the existing localization schemes by significant margin at all measured and simulated locations. However, the VRD based localization does not mention how to match the estimated VRD with the measured one-bound path and it requires both transceivers with the ability of measuring TOA and AOA which is an expensive approach. This section presents a VRD based TOA localization algorithm with the knowledge of environment layout that overcomes above limitation.

The layout map of the environment is shown in Fig. 9.5, where the solid line is the boundary of the enclosed room and VRD_i^j represents the j^{th} VRD of RD_i. The star represents one of the MD locations in experiment. In this proposed scheme, the VRD under one-bound and two-bounds are taken into account and higher reflections are neglected.

Suppose in a cooperative manner, the time synchronization issue has been solved. The measured TOA at RD_i and traced to VRD_i^j can be represented as

$$R_i^j = d_i^j + \varepsilon_i^j = \sqrt{\left(x - x_i^j\right)^2 + \left(y - y_i^j\right)^2} + \varepsilon_i^j , \tag{9.7}$$

where $\boldsymbol{p} = (x, y)$ and $\boldsymbol{p}_i^j = \left(x_i^j, y_i^j\right)$ represent the position of RD and VRD, respectively. And ε_i^j represents the Gaussian distributed ranging error with zero mean and standard deviation (std) of σ_i^j.

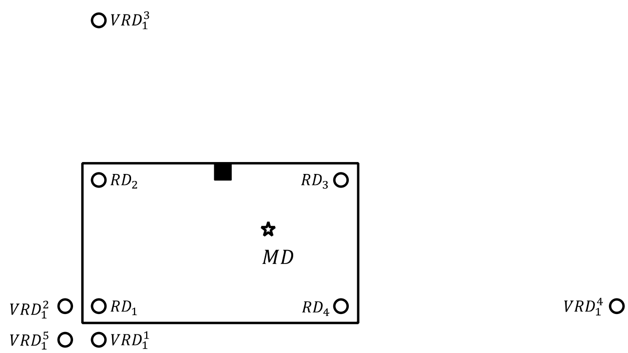

Fig. 9.5. Layout map of the environment, where VRD_i^j represents the j^{th} VRD of RD_i.

Furthermore, some measurements for each RD cannot be traced to any VRD and may come from other scatterers such as ceilings and floors. These scatterers are not considered in the model, and the generated measurements are treated as clutter, which is denoted as R_i^c for clutter received at RD_i. The R_i^c follows a uniform distribution [31]

$$R_i^c \sim U\left[0, R_{max}\right], \tag{9.8}$$

where R_{max} is the maximum value for the range measurement, which is selected to be sufficiently greater than the maximum possible distance to any VRD. It should also be noted that some LOS or reflection paths in the real environment may be blocked by obstructers, which means that some VRDs cannot be assigned any measurement. Therefore, the TOA measured at RD_i, denoted as $\tilde{R}_i$, contains two types of measurements: effective measurements (unblocked LOS and reflection paths) and clutter. To localize the MD, the data association process should be performed to filter out the clutter and estimate the correct association between the measurements and the corresponding VRDs.

9.4.2. Two-step Weighted Least Squares Localization

Suppose that the data association has been performed, the clutter has been filtered out, and the correct association result is estimated. The MD can be localized with a two-step weighted least squares algorithm using associated paths, which will be summarized as follows. Square both side of (9.7) we can get

$$(R_i^j)^2 = K_i^j - 2x_i^j x - 2y_i^j y + x^2 + y^2, \tag{9.9}$$

where $K_i^j = \left(x_i^j\right)^2 + \left(y_i^j\right)^2$. By introducing $R^2 = x^2 + y^2$, (9.9) can be linearized as

$$-2x_i^j x - 2y_i^j y + R^2 + K_i^j = (R_i^j)^2 \tag{9.10}$$

By defining $\boldsymbol{p_a} = \left[x, y, R^2\right]^T$, and assuming R^2 is independent of x and y, (9.10) can be arranged in matrix form as

$$\mathbf{A_i p_a} + \mathbf{K_i} = \mathbf{b_i}, \tag{9.11}$$

where

$$\mathbf{A_i} = \begin{pmatrix} -2x_i^0 & -2y_i^0 & 1 \\ -2x_i^1 & -2y_i^1 & 1 \\ \vdots & \vdots & \vdots \\ -2x_i^M & -2y_i^M & 1 \end{pmatrix}, \mathbf{K_i} = \begin{pmatrix} (K_i^0)^2 \\ (K_i^1)^2 \\ \vdots \\ (K_i^M)^2 \end{pmatrix}, \mathbf{b_i} = \begin{pmatrix} (R_i^0)^2 \\ (R_i^1)^2 \\ \vdots \\ (R_i^M)^2 \end{pmatrix},$$

where M is the number of VRDs taken into account. It should be noted that (9.11) considers perfect data association. To incoporate the data association, the data association matrix is introduced and (9.11) can be expressed as

$$\boldsymbol{\varphi}_\mathbf{i} = \mathbf{P_i^1 Z_i} - \mathbf{P_i^2}(\mathbf{A_i p_a} + \mathbf{K_i}), \tag{9.12}$$

$$\boldsymbol{Z_i} = \begin{pmatrix} (\tilde{R}_i^1)^2 \\ (\tilde{R}_i^2)^2 \\ \vdots \\ (\tilde{R}_i^{N_i})^2 \end{pmatrix}, \boldsymbol{\varphi_i} = \begin{pmatrix} 2R_i^1\varepsilon_i^1 + \left(\varepsilon_i^1\right)^2 \\ 2R_i^2\varepsilon_i^2 + \left(\varepsilon_i^2\right)^2 \\ \vdots \\ 2R_i^{L_i}\varepsilon_i^{L_i} + \left(\varepsilon_i^{L_i}\right)^2 \end{pmatrix},$$

where $\boldsymbol{P_i^1}$ and $\boldsymbol{P_i^2}$ are $L_i \times N_i$ and $L_i \times \left(1 + M_i\right)$ data association matrix, respectively, where $L_i = \min\left(N_i, \left(1 + M_i\right)\right)$. The process of determination of data association matrix $\boldsymbol{P_i^1}$ and $\boldsymbol{P_i^2}$ is the data association process which would be illustrated later. The $\boldsymbol{\varphi_i}$ represents the noise term. Then the $\boldsymbol{p_a}$ can be estimated as

$$\hat{\boldsymbol{p}}_a = \arg \min_{\boldsymbol{p}_a,\, \boldsymbol{P}_i^1,\, \boldsymbol{P}_i^2} E\left[\boldsymbol{\varphi}^T \boldsymbol{\Psi}^{-1} \boldsymbol{\varphi}\right], \tag{9.13}$$

where $\boldsymbol{\varphi} = \left[\boldsymbol{\varphi}_1, \boldsymbol{\varphi}_2, \boldsymbol{\varphi}_3, \boldsymbol{\varphi}_4\right]^T$ and $\boldsymbol{\Psi} = \mathrm{diag}\left\{\boldsymbol{\Psi}_1, \ldots, \boldsymbol{\Psi}_4\right\}$ where $\boldsymbol{\Psi}_i = \boldsymbol{E}\left[\boldsymbol{\varphi}_i \boldsymbol{\varphi}_i^T\right] = 4\boldsymbol{B}_i \boldsymbol{Q}_i \boldsymbol{B}_i$, $\boldsymbol{B}_i = diag\left\{\boldsymbol{R}_i^1, \ldots \boldsymbol{R}_i^{L_i}\right\}$, $\boldsymbol{Q}_i = \mathrm{diag}\left\{(\sigma_i^0)^2, \ldots, (\sigma_i^{L_i})^2\right\}$.

And the covariance matrix of $\boldsymbol{p}_a$ can be given as $\mathrm{cov}(\mathbf{p}_a) = (\mathbf{G}^T \boldsymbol{\Psi}^{-1} \mathbf{G})^{-1}$, where $\boldsymbol{G} = \begin{pmatrix} \boldsymbol{G}_1 & \boldsymbol{G}_2 & \boldsymbol{G}_3 & \boldsymbol{G}_4 \end{pmatrix}^T$ and $\boldsymbol{G}_i = \boldsymbol{P}_i^2 \boldsymbol{A}_i$. It should be noted that the data association matrix $\boldsymbol{P}_i^1$ and $\boldsymbol{P}_i^2$ should be estimated simultaneously with $\boldsymbol{p}_a$ due to the system does not have any prior knowledge about MD. After estimated $\boldsymbol{p}_a$, the final position of MD can be estimated followed as [32]. In the next section, we focused on how to estimate the data association matrix $\boldsymbol{P}_i^1$ and $\boldsymbol{P}_i^2$.

9.4.3. Proposed Grid-based Data Association

In this section, the grid-based data association algorithm is proposed to estimate the data association matrix. A given accurate floor plan can be divided into grid points. At each grid point, a set of noiseless path lengths to each RD and VRD can be calculated denoted as $\boldsymbol{R}_i$. Suppose the measured data set denoted as $\tilde{\boldsymbol{R}}_i$, the element in $\tilde{\boldsymbol{R}}_i$, denoted as $\tilde{R}_i^k$, and element in $\boldsymbol{R}_i$ denoted as R_i^j. Then, at each grid point, the data association process is to assign the elements in $\tilde{\boldsymbol{R}}_i$ to the elements in $\boldsymbol{R}_i$ and make the overall difference minimum. Then this data association process can be expressed as

$$\langle \tilde{R}_i^k, R_i^j \rangle = \arg\min_{j,k} \left|\tilde{R}_i^k - R_i^j\right|, \text{ subject to}: \left|\tilde{R}_i^k - R_i^j\right| < d_t, \tag{9.14}$$

where $\langle \tilde{R}_i^k, R_i^j \rangle$ represents the k^{th} observation is associated with the j^{th} path. And d_t is a threshold used to reject the observation-to-path pair with large distance difference. The threshold d_t called cut-off distance, usually selected as two to three times of σ_i^0 [33]. To determine the data association matrix $\boldsymbol{P}_i^1$ and $\boldsymbol{P}_i^2$ at each grid point, the data association process should be iterative performed L_i times. For l^{th} iteration, if there is a set $\tilde{R}_i^k$, R_i^j satisfies (9.14) which means associated, then the k^{th} column of l^{th} row of $\boldsymbol{P}_i^1$ and j^{th} column of l^{th} row of $\boldsymbol{P}_i^2$ would be assigned to '1'. Otherwise, the l^{th} row of both $\boldsymbol{P}_i^1$ and $\boldsymbol{P}_i^2$ are zeros. It should be noted that each measurement and path can only be associated once, then each row and column in both data association matrices have at most a single 1. Some rows in both data association matrices may contain only 0. A row of all zeros in $\boldsymbol{P}_i^2$ means that the corresponding path is blocked so that no measurement is associated with it. Similarly, a row of all zeros in $\boldsymbol{P}_i^1$ indicates that the corresponding measurement is a clutter, so no path is associated with it.

At each grid point, we can perform data association and calculate the mean square residual $E\left[\boldsymbol{\varphi}^T \boldsymbol{\Psi}^{-1} \boldsymbol{\varphi}\right]$ using (9.13). The possible MD position will then be considered near the grids with the minimum square residual. The final estimation of $\boldsymbol{P}_i^1$ and $\boldsymbol{P}_i^2$ can then be determined by performing data association at the centroid of H grids with the minimum square residual. After estimated the data association matrix, the MD can be localized using the two-step weighted least square method introduced above.

9.5. Simulation Result for VRD Based TOA Localization

To evaluate the performance of our proposed VRD based TOA localization algorithm, simulation and experiment were performed in the environment as shown in Fig. 9.5. The environment was a closed meeting room environment with dimensions of 8.3 m × 7.3 m in the INFINITUS laboratory at the School of EEE, Nanyang Technological University (NTU). Four RDs are placed at the corners of the meeting room with coordinates of (1.4, 1), (1.4, 6.3), (7.1, 6.1), and (7.3, 1) respectively. The MD is placed at a 4 × 4 rectangular grids with 1 m intervals between each grid, for a total of 16 positions, with coordinates from (2.4, 2) to (5.4, 5).

We considered four situations to compare. The first situation, which considers only LOS paths with perfect data association results, is called LOS- PDA. The second situation, which considers both LOS and NLOS paths with perfect data association results, is called multipath-PDA. The LOS-PDA and the multipath- PDA are both used as benchmarks. The third situation, which considers only the LOS path but assumes that the shortest path is the LOS path, is called LOS-DA. The fourth situation, which considers both LOS and NLOS paths but requires data association to associate multipath components with their corresponding VRDs, is called multipath-DA. The number of grids, H, with the minimum square residual used to estimate the final association matrices is set to 6.

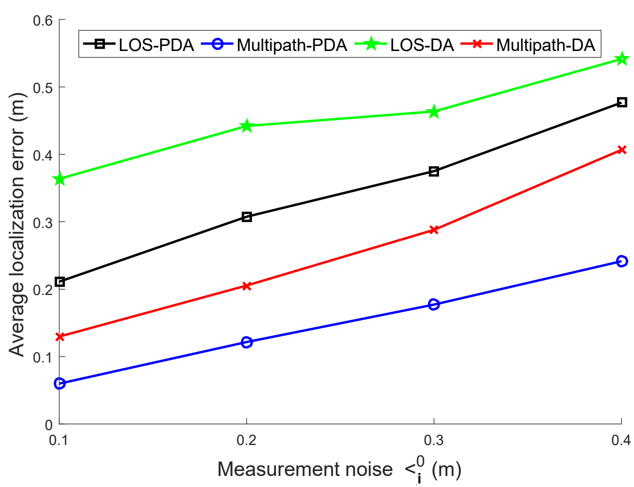

Fig. 9.6. Comparison of average localization error (ALE) with different levels of measurement noise σ_i^0.

The performance comparison of the proposed algorithms with different levels of measurement noise σ_i^j was given. The measurement noise of LOS path σ_i^0 varied from 0.1 m to 0.4 m. To account for the reflection loss, the measurement noises of the reflection paths are doubled for each reflection, which means that the measurement noises of the single and double reflection paths were $2\sigma_i^0$ and $4\sigma_i^0$, respectively. Each algorithm was reiterated 25 times using different random sequences to generate measurements. The probability for a path been blocked is set as 0.9. The pillar shown in Fig. 9.5 was considered to be a point scatterer that generates clutter. The average localization error (ALE) of the MD are presented in Fig. 9.6. The multipath-DA achieved ALE between 0.15 m and 0.4 m when σ_i^0 was varied from 0.1 m to 0.4 m. The multipath-DA performs even better than the LOS-PDA because the number of LOS paths is insufficient to localize the MD at some points. This result shows the ability of the proposed multipath-DA to work in situations with an insufficient number of LOS paths.

9.6. Conclusion

We have presented a novel NLOS localization scheme based on the concept of virtual RD. Simulation and experimental results have shown that our proposed NLOS localization scheme using one RD outperforms the existing localization schemes by significant margin at all measured and simulated locations. Furthermore, to overcome the expensive methodology of using both TOA and AOA, another TOA-based indoor localization algorithm is presented that uses multipath components with accurate knowledge of the floor plan. The NLOS paths are associated with their corresponding VRDs with the proposed grid-based data association method. The data association process is integrated with the two-step weighted least squares method by the proposed data association matrix. The simulation result show that the proposed TOA-based indoor localization algorithm using multipath components outperformed the conventional TOA-based indoor localization algorithm using LOS only in terms of localization accuracy.

References

[1]. G. Seco-Grandados, J. A. Lopez-Salcedo, D. Jimenez-Banos, G. Lopez-Risueno, Challenges in indoor global navigation satellite systems: unveiling its core features in signal processing, *IEEE Signal Processing Magazine*, Vol. 29, March 2012, pp. 108-131.

[2]. Y. Jin, W-S. Soh, M. Motani, W-C. Wong, A robust indoor pedestrian tracking system with sparse infrastructure support, *IEEE Trans. Mobile Computing*, Vol. 12, Issue 7, July 2013, pp. 1392-1403.

[3]. P. Bahl, V. Padmanabhan, RADAR: An in-building RF based user location and tracking system, in *Proceedings of the IEEE International Conference on Computer Communications (INFOCOM'2000)*, 2000, pp. 775-784,

[4]. Z. Deng, Y. Yu, X. Yuan, N. Wan, L. Yang, Situation and development tendency of indoor positioning*, China Communications,* Vol. 10, Issue 3, March 2013, pp. 42-55.

[5]. S. He, S. Chan, Wi-Fi fingerprint-based indoor positioning: recent advances and comparisons, *IEEE Commun. Surveys & Tutorials*, Vol. 18, Issue 1, August 2015, pp. 466-490.

[6]. H. Liu, H. Darabi, P. Banerjee, J. Liu, Survey of wireless indoor positioning techniques and systems, *IEEE Trans. Syst. Man Cybern*. C, *Appl. Rev*., Vol. 37, Issue 6, November 2007, pp. 1067-1080.
[7]. X. Wang, Z. X. Wang, B. O'Dea, A TOA-based location algorithm reducing the errors due to Non-Line-of-Sight (NLOS) propagation, *IEEE Trans. Vehicular Technology*, Vol. 52, Issue 1, January 2003, pp. 112-116.
[8]. S. Kay, N. Vankayalapati, Improvement of TDOA position fixing using the likelihood curvature, *IEEE Trans. Signal Processing*, Vol. 61, Issue 8, April 2013, pp. 1910-1914.
[9]. K. Yu, E. Dutkiewicz, Geometry and motion-based positioning algorithm for mobile tracking in NLOS environments, *IEEE Trans. Mobile Computing*, Vol. 11, Issue 2, February 2012, pp. 254-263.
[10]. L. Lu, H-C. Wu, Novel robust direction-of-arrival-based source localization algorithm for wideband signals, *IEEE Trans. Wireless Comm*., Vol. 11, Issue 11, November 2012, pp. 3850-3858.
[11]. L. Cong, W. H. Zhuang, Hybrid TDOA/AOA mobile user location for wideband CDMA cellular systems, *IEEE Trans. Wireless. Comm*., Vol. 1, Issue 3, July 2002, pp. 439-447.
[12]. S. W. Chen, C. K. Seow, S. Y. Tan, Single reference mobile localisation in multipath environment, *IEE Electronics Letters,* Vol. 49, Issue 21, October 2013, pp. 1360-1362.
[13]. C. K. Seow, S. Y. Tan, Localisation of mobile device in multipath environment using bi-directional estimation, *IEE Electronics Letters,* Vol. 44, Issue 7, March 2008, pp. 485-487.
[14]. S. W. Chen, S. Y. Tan, C. K. Seow, Peer-to-peer localization in urban and indoor environments, *Progress in Electromagnetics Research B,* Vol. 33, 2011, pp. 339-358.
[15]. S. Y. Tan, H. S. Tan, Modelling and measurements of channel impulse response for an indoor wireless communication system, *IEE Proc.-Microw. Antennas Propag.,* Vol. 42, Issue 5, October 1995, pp. 405-410.
[16]. X. Wang, Z. Wang, B. O'Dea, A TOA-based location algorithm reducing the errors due to non-line-of-sight (NLOS) propagation, *IEEE Trans. Veh. Technol*., Vol. 52, Issue 1, January 2003, pp. 112-116.
[17]. N. Khajehnouri, A. Sayed, A non-line-of-sight equalization scheme for wireless cellular location, in *Proceedings of the IEEE Int. Conference Acoust., Speech, Signal Process. (ICASSP'03),* Hong Kong, April 2003, pp. 549-552.
[18]. T. Jia, R. M. Buehrer, A set-theoretic approach to collaborative position location for wireless networks, *IEEE Trans. Mobile Computing*, Vol. 10, Issue 9, September 2011, pp. 1264-1275.
[19]. L. Cong, W. H. Zhung, Nonline-of-sight error mitigation in mobile location, *IEEE Trans. Wireless Commun.*, Vol. 4, Issue 2, March 2005, pp. 560-573.
[20]. Y. Chan, W. Tsui, H. So, P. Ching, Time-of-arrival based localization under NLOS conditions, *IEEE Trans. Veh. Technol*., Vol. 55, Issue 1, January 2006, pp. 17-24.
[21]. J. Li, J. Conan, S. Pierre, Mobile terminal location for MIMO communication systems, *IEEE Trans. Antennas and Propagation*, Vol. 55, Issue 8, August 2007, pp. 2417-2420.
[22]. C. K. Seow, S. Y. Tan, Non-Line-of-Sight localization in multipath environments, *IEEE Trans. Mobile Computing*, Vol. 7, Issue 5, May 2008, pp. 647-660.
[23]. S. W. Chen, C. K. Seow, S. Y. Tan, Virtual reference device-based NLOS localization in multipath environment, *IEEE Antennas and Wireless Propagation Letters*, Vol. 13, July 2014, pp. 1409-1412.
[24]. E. Leitinger, M. Fröhle, P. Meissner, K. Witrisal, Multipath-assisted maximum-likelihood indoor positioning using UWB signals, in *Proceedings of the IEEE International Conference on Communications (ICC'14*), Sydney, June 2014, pp. 170-175.
[25]. D. Liu, K. Liu, Y. Ma, J. Yu, Joint TOA and DOA localization in indoor environment using virtual stations*, IEEE Commun. Lett.,* Vol. 18, Issue 8, June 2014, pp. 1423-1426.

[26]. K. Witrisal, P. Meissner, Performance bounds for multipath-assisted indoor navigation and tracking (MINT), in *Proceedings of the IEEE International Conference on Communications (ICC'12*), Ottawa, June 2012, pp. 4321-4325.
[27]. L. Li, J. Krolik, Simultaneous target and multipath positioning, *IEEE J. Sel. Topics Signal Process.*, Vol. 8, Issue 1, November 2013, pp. 153-165.
[28]. G. Strang, Linear Algebra and Its Application, *Thomson*, Belmont, 2006.
[29]. Z-J. Hossein, P. Subbarayan, EM-based recursive estimation of channel parameters, *IEEE Trans. Communications*, Vol. 47, Issue 9, September 1999, pp. 1297-1302.
[30]. S. Y. Tan, H. S. Tan, Improved three dimensional ray tracing technique for microcellular propagation models, *IEE Electronics Letters,* Vol. 31, Issue 17, August 1995, pp. 1503-1505.
[31]. B. Vo, W. Ma, The Gaussian mixture probability hypothesis density filter, *IEEE Trans. Signal Process*., Vol. 54, Issue 11, November 2006, pp. 4091-4104.
[32]. H. Zhang, C. K. Seow, S. Y. Tan, Virtual reference device-based narrowband TOA localization using LOS and NLOS path, in *Proceedings of the IEEE/ION Position, Location and Navigation Symposium (PLANS'16)*, April 2016, pp. 225-231.
[33]. P. Meissner, E. Leitinger, M. Froehle, K. Witrisal, Accurate and robust indoor localization systems using ultra-wideband signals, in *Proceedings of the European Navigation Conference (ENC'13),* Vienna, 2013.

Advances in Networks, Security and Communications: Reviews, Volume 2

Sergey Y. Yurish, Editor

Written by 31 contributors from academy and industry from 12 countries (Austria, Bulgaria, China, Croatia, Germany, India, Iran, Singapore, South Korea, Taiwan, UK and USA) the book contains 14 chapters divided into three main parts: Networks (six chapters), Communications (seven chapters) and Security (one chapter). With this unique combination of information in each volume, the *'Advances in Networks, Security and Communications: Reviews'* Book Series will be of value for scientists and engineers in industry and universities.

Like the first volume of this book Series, the second volume also has been organized by topics of high nterest. In order to offer a fast and easy reading of the state of the art of each topic, every chapter in this book is independent and self-contained.

This book ensures that our readers will stay at the cutting edge of the field and get the right and effective start point and road map for the further researches and developments. By this way, they will be able to save more time for productive research activity and eliminate routine work.

This book will be a valuable tool in both learning how to design various networks, as well as a reference as an advance in readers' research careers.

IFSA

ISBN 978-84-09-14509-6

9 788409 145096